

Interaction between EMI Filter and Power Factor Preregulators with Average Current Control: Analysis and Design Considerations

Giorgio Spiazzi

Dept. of Electronics and Informatics - University of Padova
Via Gradenigo 6/a 35131 - Padova - Italy
e-mail: giorgio@tania.dei.unipd.it

José Antenor Pomilio

School of Electrical and Computer Eng. – Univ. of Campinas
C.P. 6101 13081-970 - Campinas – Brazil
e-mail: antenor@dsce.fee.unicamp.br

Abstract - The effects of a non negligible source impedance, due to the presence of an input EMI filter, on the stability of Power Factor Preregulators with average current control are analyzed by using a State Space Averaged model. The modeling allows to derive a simple expression for the loop gain in terms of the converter current loop gain. The overall system stability is studied for boost, Cuk and SEPIC PFP topologies. Based on this model, a simple modification of the standard current control loop is proposed which increases the converter robustness. Comparison between model forecasts and experimental measurements is carried out using two prototypes: one based on the boost topology and the other based on the SEPIC topology both rated at 600W. Finally, the model accuracy is investigated with measurements at different current loop bandwidths.

I. INTRODUCTION

Owing to an increased necessity for harmonic line current reduction, high power factor ac-dc converters (also called Power Factor Preregulators - PFP's) are becoming an important issue in modern electric energy power conversion systems. In particular, limiting standards like IEC 1000-3-2, which have become effective since January 1996, impose maximum values for current harmonics drawn from the utility grid [1]. Thus, in the last five years, we assisted to a proliferation of topologies and control techniques which perform an input current shaping so that to increase the power factor [2-8]. Among them, the boost converter working in Continuous Conduction Mode (CCM) with average current control is probably one of the most popular solution for single-phase PFPs thanks to its simplicity, low input current ripple and availability on the market of many control IC's. Moreover, the design of such converter is broadly described in many papers [2,3]. The same control technique can also be applied to other topologies with an input inductor like Cuk and SEPIC which, differently from the boost, feature high-frequency isolation, step-up and step-down capability, inherent short circuit and overcurrent protection, input current high frequency ripple reduction through magnetic coupling, etc. [7]. The power factor achievable with this structures is actually very high and can approach unity.

However, such converters produce high frequency noise due to the switching action that must be filter out in order to comply with EMI standards like IEC CISPR series. In order

to do this, an external EMI input filter is generally used between the line grid and the PFP. When the EMI filter is added, instabilities can arise in the system due to the interaction between the filter and the converter. This phenomenon is well known and many papers have already addressed it [10-13]. Different from those references, [14] reports an analysis, for the boost converter, in which the derived loop gain provides an easy insight into the PFP design.

The main contribution of this paper is the extension of such analysis to other PFP topologies with average current control, like Cuk and SEPIC. Moreover, the results of the proposed analysis suggest a simple modification in the inner current loop of the average current control which allows to greatly improve the converters robustness against filter-induced instabilities.

Two prototype converters were built in order to validate the theoretical analysis: a boost and a SEPIC PFPs both rated at 600W. The experimental measurements done show a good correspondence between model forecasts and actual converters behavior.

II. FILTER-CONVERTER INTERACTION ANALYSIS

In order to show the nature of the problem let us start with a boost PFP whose simplified scheme with average current mode control is shown in fig.1 together with the EMI input filter. As we can see, the core of the input current shaping is an inner current loop which forces the measured inductor current to follow a suitable reference signal I_{REF} . The latter is built by sensing the rectified input voltage u_g (block k in fig.1 is a scaling factor) and by multiplying it with the output u_c of the voltage-error amplifier of the external output voltage loop. This signal is practically constant at frequencies above the line frequency since the voltage loop has a bandwidth much lower than the line frequency in order to maintain a good power factor. Thus u_c sets the correct current reference amplitude in order to maintain the regulation of the output voltage. It is worthy to note that the same control structure is used with Cuk and SEPIC PFPs. The same figure also shows the circuit model which represents the interface between the filter and the converter in which the Thevenin equivalent circuit of the filter output was used (H_F is the filter attenuation). We can write:

This work was supported by CNPq. Dr. Spiazzi visit to the University of Campinas was supported by FAPESP.

$$\frac{u_g}{u_i} = \frac{H_F}{1 + \frac{Z_{OF}}{Z_{IC}}} = \frac{H_F}{1 + T_F} \quad (1)$$

$$T_F = \frac{Z_{OF}}{Z_{IC}} = Z_{OF} Y_{IC} \quad (2)$$

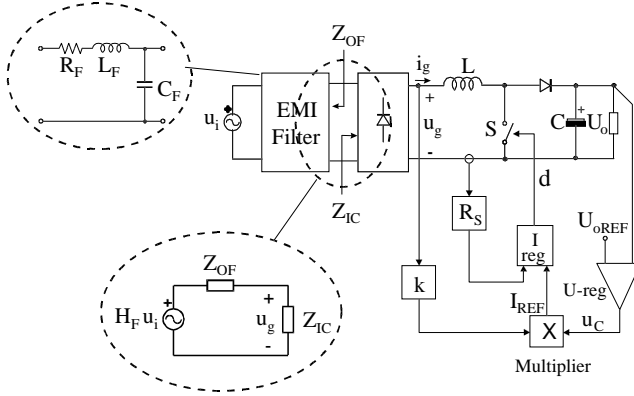


Fig.1- Basic scheme of a boost PFP with average current control plus an input EMI filter

T_F can be interpreted as a loop gain which must satisfy the Nyquist criterion for stability. If $|T_F(j\omega)|$ were always lower than one, no instabilities could arise in the system and this sufficient criterion was largely used in the past, especially for dc-dc converters [10,11]. However, in the case of ac-dc converters with high power factor, limitations exist both on the filter component values and on the converter design [9]. Thus we will see that it is quite common to have $|T_F(j\omega)| > 1$ in a frequency range above the inner current loop crossover frequency, especially at low line voltage and high load currents, and in this case the general approach for stability analysis must be followed. Thus, from (2), we see that the knowledge of the converter input admittance is a prerequisite for the stability analysis.

In the following section this input admittance will be derived for boost, Cuk and SEPIC converters. To this purpose it is important to observe that in this analysis the output voltage U_o can be considered constant owing to the high value of the output filter capacitor needed to filter out the low frequency components of the fluctuating input power.

III. PFP'S INPUT ADMITTANCE

The calculation of the input impedance (or admittance) of boost, Cuk and SEPIC converters follows two steps:

1-from the scheme of fig.1 the relation imposed by the controller between duty-cycle and input voltage and current perturbations is derived as follows:

$$\hat{d} = K_u(s) \hat{u}_g + K_i(s) \hat{i}_g + K_c(s) \hat{u}_c \approx K_u(s) \hat{u}_g + K_i(s) \hat{i}_g \quad (3)$$

where hat means perturbations respect to steady-state

values. It was considered $\hat{u}_c = 0$, and consequently u_c is constant at the frequency range we are interested in.

2-from the converter small signal model the relation between input current, duty-cycle and input voltage perturbations is derived as follows:

$$\hat{i}_g = Y_{HF}(s) \hat{u}_g + G_{id}(s) \hat{d} + C(s) \hat{u}_c \approx Y_{HF}(s) \hat{u}_g + G_{id}(s) \hat{d} \quad (4)$$

The symbol Y_{HF} was used for the first coefficient in (4) because it represents the high frequency converter input admittance, i.e. the admittance at frequency above the current loop crossover frequency in which d is constant. G_{id} represents the transfer function between duty-cycle and input current which is used for the current loop gain calculation. In fact, from (3) and (4) the current loop gain $T_i(s)$ can be derived, considering $\hat{u}_g = 0$, as:

$$T_i(s) = -G_{id} K_i(s) \quad (5)$$

A. Controller analysis

From the analysis reported in the Appendix, which refers to a standard average current controller IC like the UC3854 or the L4981, the expression for coefficients $K_u(s)$ and $K_i(s)$ are derived as follows:

$$K_i(s) = -\frac{R_S}{U_{OSC}} G_{ri}(s) \quad (6)$$

$$K_u(s) = -\frac{I_g}{U_g} K_i(s) = -G_{IC} K_i(s) \quad (7)$$

where R_S is the current sensing resistance, U_{OSC} is the amplitude of the controller internal ramp, $G_{ri}(s)$ is the current error amplifier transfer function and U_g and I_g are RMS input voltage and current respectively.

The current loop usually uses a PI regulator with a high frequency additional pole in order to reject the high-frequency input current ripple (see Fig.A1), i.e.

$$G_{ri}(s) = I + \frac{\omega_{ri}}{s} \left(\frac{I + s\tau_{zi}}{I + s\tau_{pi}} \right) \quad (8)$$

Using (3-7) a general expression for the PFP input admittance independent of the particular topology can be found as

$$Y_{IC}(s) = Y_{HF}(s) \frac{I}{I + T_i(s)} + G_{IC} \frac{T_i(s)}{I + T_i(s)} \quad (9)$$

From this expression, we can see that at frequencies below the current loop bandwidth ($|T_i(j\omega)| \gg 1$) the input admittance is constant and equal to G_{IC} , while at frequency above the current loop crossover frequency ($|T_i(j\omega)| \ll 1$) it coincides with Y_{HF} . From (7) we see that the low-frequency input admittance G_{IC} depends on the converter operating point, i.e.

$$G_{IC} = \frac{I_g}{U_g} = \frac{P_o}{U_g^2} \quad (10)$$

where P_o is the output power. From (10) we can see that the low-frequency converter input impedance decreases at high power and low input voltage thus making the system more susceptible to instabilities induced by filter-converter interactions.

B. Boost PFP

The derivation of (4) for the boost converter is done starting from the well known state space average model shown in fig.2a) for CCM operation. In this figure $d'=1-d$ is the complement of the duty-cycle. Since the output voltage U_o can be considered constant, the model can be simplified as shown in fig.2b). From it we can easily derive:

$$\hat{i}_g = \frac{I}{sL} \hat{u}_g + \frac{U_o}{sL} \hat{d} \quad (11)$$

Consequently, the expressions for the current loop gain $T_i(s)$ and high-frequency input admittance $Y_{HF}(s)$ become respectively:

$$T_i(s) = \frac{U_o}{sL} \cdot \frac{R_s}{U_{osc}} \cdot G_{ri}(s) \quad (12)$$

$$Y_{HF}(s) = \frac{I}{sL} \quad (13)$$

An important conclusion is that the input impedance for the boost converter does not depend on the instantaneous input voltage but only on its RMS value through G_{IC} .

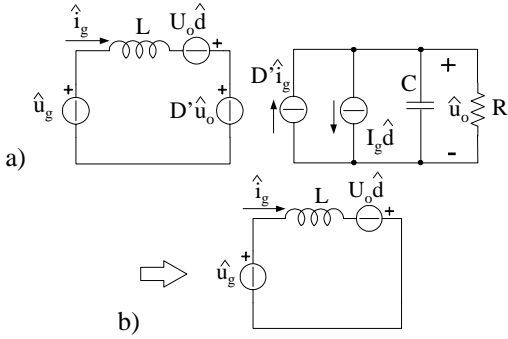


Fig.2- a) State space average model of boost converter in CCM; b) simplified model for input impedance calculation

C. Cuk and SEPIC PFPs

The basic schemes of ac-dc converters employing Cuk and SEPIC topologies are reported in fig. 3. Note the damping network across the energy transfer capacitor C_1 (R_d - C_d) used in order to smooth the converter transfer functions as suggested in [7]. The input admittance calculation makes use of the PWM switch model [15]. The simplified small signal

model which results short circuiting the output filter capacitor is the same for both topologies and is shown in fig. 3c). From it, expression for $Y_{HF}(s)$ and $G_{id}(s)$ are easily derived as follows:

$$G_{id}(s) = DU_D \frac{L'}{L_2 L_1} \left\{ \frac{1 + s \left(\frac{I_C}{U_D} \frac{D'}{D} L_2 + \tau_d \right)}{s \left(1 + s \tau_d + s^2 L' (C_1 + C_d) + s^3 L' C_1 \tau_d \right)} + \frac{s^2 \frac{L_2}{D} \left(C_1 + C_d + \frac{I_C}{U_D} D' \tau_d \right) + s^3 \frac{L_2 C_1}{D} \tau_d}{s \left(1 + s \tau_d + s^2 L' (C_1 + C_d) + s^3 L' C_1 \tau_d \right)} \right\} \quad (14)$$

$$Y_{HF}(s) = \frac{I}{s L_1 \left(1 + \frac{D'^2 L_2}{D^2 L_1} \right)} \frac{1 + s \tau_d + s^2 \frac{L_2}{D^2} (C_1 + C_d) + s^3 \frac{L_2 C_1}{D^2} \tau_d}{\left(1 + s \tau_d + s^2 L' (C_1 + C_d) + s^3 L' C_1 \tau_d \right)} \quad (15)$$

where $U_D(\theta) = u_g(\theta) + U_o$ and $I_C(\theta) = i_g(\theta) + i_2(\theta)$ are parameters which, together with the duty-cycle, depend on the converter instantaneous operating point, i.e. on the line angle $\theta = \omega_1 t$. The parameter L' is given by:

$$L'(\theta) = \frac{L_1 L_2}{D^2 L_1 + D'^2 L_2} \quad (16)$$

Expressions without the damping network can be easily derived letting $C_d=0$ in (14) and (15).

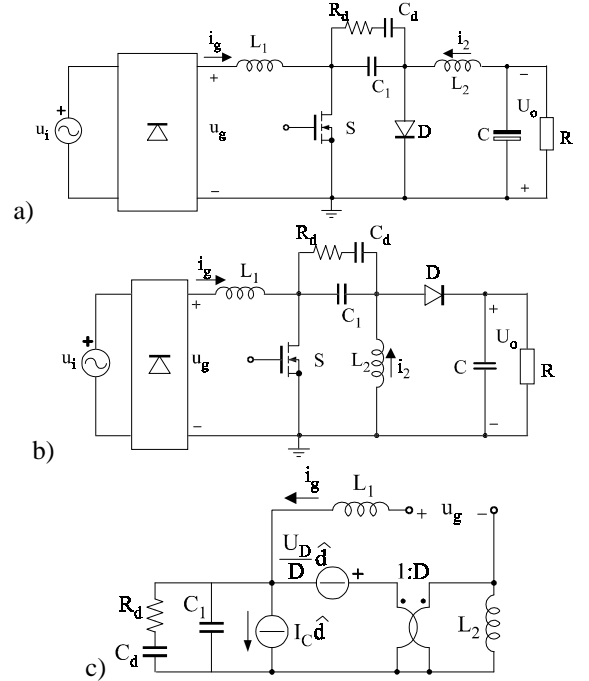


Fig. 3- Basic PFP topologies; a) Cuk; b) SEPIC; c) small signal model for input impedance calculation

IV. MODEL PREDICTIONS

From (1) and (9) we are now able to predict the high frequency instabilities which can occur from the filter-converter interaction. Let us consider for example a SEPIC PFP with a simple single-cell EMI filter as shown in fig.1. The converter and controller parameters are reported in Table II while the filter parameters are: $R_F=1\Omega$, $L_F=0.55\text{mH}$, $C_F=470\text{nF}$. The bode plot of the resulting loop gain $T_F(j\omega)$ is shown in fig.7 (left) for two different input voltage values and rated output voltage and power. As we can see, at lower input voltage the system results unstable since at the crossover frequency $f_{ca}=20\text{kHz}$ (see curve a)) the phase margin is -8 degrees, while at higher input voltage it become stable (at $f_{cb}=18\text{kHz}$ the phase margin is about $+15$ degrees. These curves are obtained at an operating point corresponding to the peak of the input voltage (line angle $\theta=\pi/2$). The dependence of loop gain $T_F(j\omega)$ on the line angle θ is shown in fig.7 (right) where the same minimum input voltage was used with two different line angles θ (curve a) $\theta=\pi/2$, curve b) $\theta=\pi/200$). In this case the worst condition corresponds to the peak of the input voltage.

V. EXPERIMENTAL RESULTS

In order to test the validity of the model forecasts two prototypes were built and tested. The first one is based on the boost topology and its parameter values are reported in Table I, while the second one employs a SEPIC converter whose parameter values are reported in Table II. Both converters are supplied from the utility grid using an isolating transformer plus an autotransformer in order to vary the converter input voltage. The output inductance of the supply line, which works as a filter inductance, was measured at different voltages so has to use it in the input filter model. The latter is thus a simple single-cell R_F - L_F - C_F filter as shown in fig.1.

A. Boost prototype

With the parameter values used for current error amplifier, the current loop bandwidth varies from 5kHz to 8.3kHz in the output voltage range $U_o=180\div 300\text{V}$. Comparisons between experimental measurements of the boost PFP and model predictions are reported in Table III for different operating points. The column corresponding to the experimental measurements reports the value of peak input voltage at which instability arises together with the corresponding oscillation frequency, the column labeled MODEL I reports the same information derived from the model and the last column (MODEL II) reports the crossover frequency and the phase margin as given by the model in correspondence of the measured input voltage value in which oscillations appear. As we can see, there is a pretty good agreement between model forecasts and experimental measurements.

The value used in the model for R_F was the DC value equal

to 0.9Ω . However, in this case the model is not much sensible to the value of this resistance. For example, using a non linear R_F value of the type $R_F(f)=0.9+0.1\sqrt{f}$ so as to better model the skin effect in the equivalent input filter only small variations of the values reported in Table III were observed (some model predictions become more accurate like the N°.1 for which m_ϕ becomes 0.02deg , and other become less accurate like the N°.6 for which m_ϕ becomes 7.2deg).

B. SEPIC prototype

In the case of the SEPIC PFP, the current loop bandwidth depends on the instantaneous input voltage value, i.e. on the line angle θ . With the parameter values listed in Table II, the current loop bandwidth ranges from 6.4kHz to 11.5kHz at nominal conditions. Measurements done on the SEPIC prototype at different operating points are reported in Table IV together with the model forecasts. Once again, the given model allows to predict quite well the instability phenomenon. The fixed value of measured oscillation frequency was due to measurement limitations (the oscillation period ranges from 55 to $56\ \mu\text{s}$).

VI. MODEL ACCURACY

A more careful reading of the data reported in Table III for the boost converter, reveals that the difference between measurements and model predictions depends on the output voltage value, i.e. depends on the bandwidth of the inner current loop (for Cuk and SEPIC converter the current loop bandwidth depends also on the instantaneous input voltage). In order to assess the model accuracy experimental measurements were done on the boost PFP at different current loop bandwidths. The result can be summarized as follows: the phase margin given by the model in the operating conditions in which instabilities occurs in the prototype is plotted in fig.4 against the current loop bandwidth normalized to the switching frequency. As we can see the model prediction becomes more accurate, in terms of phase margin, at lower current loop bandwidths, while the oscillation frequency prediction remains pretty good even at higher current loop bandwidths. Clearly, delays in the loops exist which are not accounted for by the simple small signal model employed.

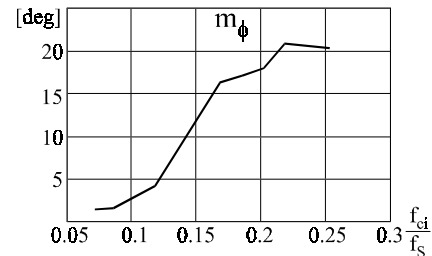


Fig.4-Model accuracy as a function of the normalized current loop bandwidth.

VII. CURRENT LOOP MODIFICATION

The derivation of expression (9) suggests a simple modification of the controller so as to increase the system robustness against instabilities. In particular, we can note that the second term at the right hand side of (9) comes from the term $K_u(s)$ in (3), i.e. from the path from u_g to I_{REF} shown in fig.1 and is the term which depends on the RMS input voltage. If we insert a low pass filter into the current reference path with a sufficiently high corner frequency so as not to appreciably degrade the rectified sinusoidal reference, then the converter input admittance $Y_{IC}(s)$ modifies as (see Appendix):

$$Y_{IC}(s) = Y_{HF}(s) \frac{I}{I + T_i(s)} + G_{IC} \frac{T_i(s)}{I + T_i(s)} \frac{I}{I + s\tau_{PB}} \quad (17)$$

Comparison between the resulting loop gain $T_F(j\omega)$ and the previous one without low-pass filter is shown in fig.5 ($f_{PB}=1/(2\pi\tau_{PB})=1.85\text{kHz}$) which refers to the SEPIC converter at $U_o=168\text{V}$ and $I_o=2.57\text{A}$. As we can see, this simple controller modification reduces the loop crossover frequency from 18kHz (f_{ca} in figure) to 13.6kHz (f_{cb} in figure) and increases the phase margin from 2.5° to 38.4° .

This low-pass filter can be inserted simply by modifying the controller scheme with the insertion of capacitor C_b as shown in Fig.A1 in Appendix.

In order to prove the efficacy of such provision, the measured input voltage and current waveforms of the SEPIC converter taken at $U_o=168\text{V}$ and $I_o=2.57\text{A}$ are reported in fig.6 which reveals the instability predicted by the loop gain $T_F(j\omega)$. Adding a low pass filter in the current reference path the system turns out to be stable in all operating conditions. The same low pass filter used with the boost converter produces the same benefits, thus eliminating the instabilities in all operating conditions, even at the higher current loop bandwidth (17kHz).

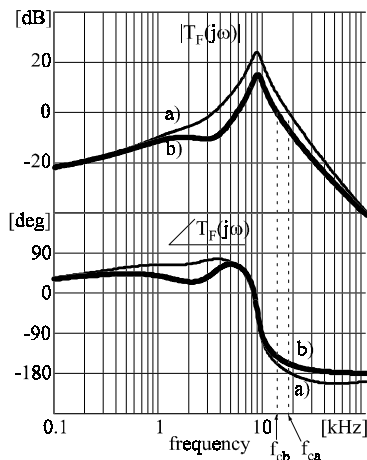


Fig.5-Gain and phase plots of loop gain $T_F(j\omega)$ for the SEPIC converter at $U_o = 168\text{V}$ and $I_o = 2.57\text{A}$; a) standard controller; b) with a low-pass filter in the current reference path ($f_{PB}=1.85\text{kHz}$)

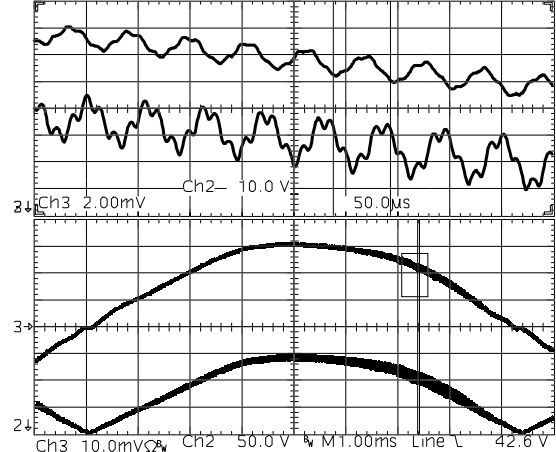


Fig.6-Experimental results of the SEPIC PFP at $U_o = 168\text{V}$ and $I_o = 2.57\text{A}$. From top to bottom: zoom of $i_g(t)$; zoom of $u_g(t)$; $u_g(t)$ 50V/div; $i_g(t)$ 2A/div.

VIII. CONCLUSIONS

In this paper the interactions between the input EMI filter, and Power Factor Preregulators with average current control are analyzed. A simple expression for the loop gain in terms of the converter current loop gain was derived for boost, Cuk and SEPIC preregulators. The derived loop gain allows useful insight into the converter controller design. In particular, based on this model, a simple modification of the standard converter current control loop is proposed which greatly increases the system robustness against instabilities induced by filter-converter interaction.

Measurements done on two prototypes demonstrated the model validity and its limitations.

REFERENCES

- [1] IEC 1000-3-2: 1995 "Electromagnetic Compatibility. Part 3: Limits - Sect. 2: Limits for harmonic current emission (equipment input current $\leq 16\text{A}$ per phase)".
- [2] Zhou, M. Jovanovic, "Design Trade-offs in Continuous Current-mode Controlled Boost Power-Factor Correction Circuits," HFPC Conf. proc., 1992, pp. 209-220.
- [3] C. Silva, "Power Factor Correction with the UC3854," Application Note, Unintegrated Circuit.
- [4] L. Balogh, R. Redl, "Power-Factor Correction with Interleaved Boost Converters in Continuous-Inductor-Current Mode," APEC Conf. Proc., 1993, pp. 168-174.
- [5] C. A. Canesin, I. Barbi, "A Unity Power Factor Multiple Isolated Outputs Switching Mode Power Supply Using a Single Switch," APEC Conf. Proc., 1991, pp. 430-436.
- [6] J. Lo Cascio, M. Nalbant, "Active Power Factor Correction Using a Flyback Topology," PCIM Conf. Proc., 1990, pp. 10-17.
- [7] G. Spiazzi, P. Mattavelli, "Design Criteria for Power Factor Preregulators Based on SEPIC and Cuk Converters in Continuous Conduction Mode," IAS Annual Meeting Conf. Proc, 1994, pp.1084-1089.
- [8] G. Spiazzi, L. Rossetto, "High-quality Rectifier based on Coupled-Inductor Sepic Topology," PESC Conf. Proc., 1994, pp. 336-341.
- [9] V. Vlatkovic, D. Borjovic, F. C. Lee, "Input Filter Design for Power Factor Correction Circuits," IEEE Trans.on Power Electronics, Vol.11, No.1, January 1996, pp.199-205.
- [10] R. D. Middlebrook, "Input Filter Considerations in Design and Application of Switching Regulators," IEEE IAS Conf. Rec., 1976, pp.366-382.

- [11] R. D. Middlebrook, "Design Techniques for Preventing Input-Filter Oscillations in Switched-Mode Regulators," Power Conversion Conf. Proc., May 4-6, 1978.
- [12] S.Y.Erich, W. M. Polivka, "Input Filter Design for Current-Programmed Regulators," IEEE APEC Conf. Proc., 1990, pp.781-791.
- [13] R. Redl, A. S. Kislovsky, "Source Impedance and Current-Control Loop Interaction in High-Frequency Power-Factor Correctors," IEEE PESC Conf. Proc., 1992, pp.483-488.
- [14] G. Spiazzi, L. Rossetto, J. A. Pomilio: "Analysis of EMI Filter Induced Instabilities in Boost Power Factor Preregulators", IEEE PESC Conf. Proc., 1998, pp. 1048-1052.
- [15] V. Vorperian, "Simplified Analysis of PWM Converters Using the Model of PWM Switch: Part I and II," IEEE Trans. on Aerospace and Elect. Systems, Vol.26, No.3, 1990, pp.490-505.

APPENDIX

From the control scheme shown in Fig. A1, which represents the standard implementation of the average current mode control (see [3]) we can derive the expression for the duty-cycle as:

$$d(\theta) = \frac{G_{ri}(s)}{U_{OSC}} (R_7 i_M(\theta) - R_S i_g(\theta)) \quad (A.1)$$

From Fig. A1, the multiplier produces an output current i_M which is given by (note that signal U_{RMS} in Fig. A1, which represents a feedforward path, is constant during a line period and thus it can be considered constant at the much higher frequencies we are interested in):

$$i_M(\theta) = \frac{u_g(\theta)}{k} u_c \quad (A.2)$$

where $k = (R_{\delta a} + R_{\delta b}) U_{RMS}^2$. At steady state, the average (in a switching period) input current is equal to its reference, i.e.:

$$R_7 I_M(\theta) = R_S I_g(\theta) \quad (A.3)$$

where uppercase means steady state conditions. Considering a perturbation around an instantaneous (during the line period) working point, from (A.2) we can obtain:

$$\hat{i}_M = \frac{U_c}{k} \hat{u}_g + \frac{U_g(\theta)}{k} \hat{u}_c = \frac{I_M(\theta)}{U_g(\theta)} \hat{u}_g + \frac{I_M(\theta)}{U_c} \hat{u}_c \quad (A.4)$$

Substituting (A.4) into (A.1) and using (A.3) we can write :

$$\hat{d} = \frac{G_{ri}(s)}{U_{OSC}} \left(R_S \frac{I_g(\theta)}{U_g(\theta)} \hat{u}_g - R_S \hat{i}_g \right) \quad (A.5)$$

from which the coefficients of (3) can be easily derived as:

$$K_i(s) = -\frac{R_S}{U_{OSC}} G_{ri}(s) \quad (A.6)$$

$$K_u(s) = -\frac{I_g(\theta)}{U_g(\theta)} K_i(s) = -\frac{I_g}{U_g} K_i(s) = -G_{IC} K_i(s) \quad (A.7)$$

where a sinusoidal input current was assumed. In this derivation we neglected capacitor C_b which is the control modification proposed in the paper. Taking it into account (A.2) modifies as

$$i_M(\theta) = \frac{u_g(\theta) u_c}{k} \frac{I}{1 + s\tau_{PB}} \quad (A.8)$$

where $\tau_{PB} = C_b \frac{R_{\delta a} R_{\delta b}}{R_{\delta a} + R_{\delta b}}$.

Consequently, (9) becomes (16).

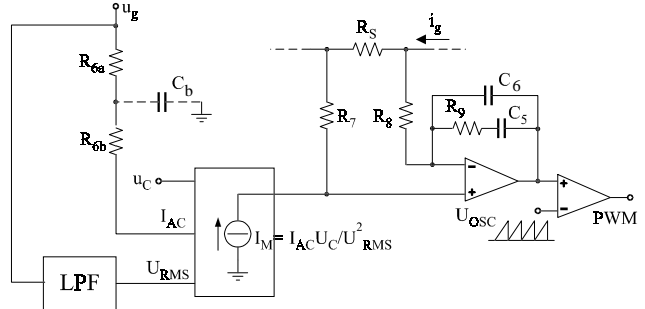


Fig. A1-Average current mode controller scheme

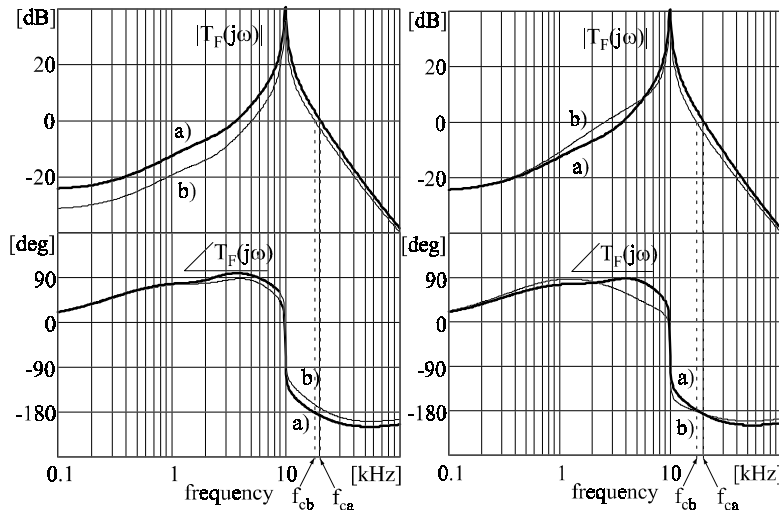


Fig.7 - Bode plots of loop gain $T_F(j\omega)$ for a SEPIC converter. Left: $\theta = \pi/2$; a) $U_g = 127V - 20\%$, b) $U_g = 127V + 20\%$. Right: $U_g = 127V - 20\%$; a) $\theta = \pi/2$, b) $\theta = \pi/200$.

TABLE I - BOOST CONVERTER PARAMETER VALUES

$U_g = 127 \text{ V}_{\text{RMS}} \pm 20\%$	$U_o = 300 \text{ V}$	$P_o = 600 \text{ W}$	$f_s = 70 \text{ kHz}$	$L = 650 \mu\text{H}$	$C = 235 \mu\text{F}$
$R_S = 33 \text{ m}\Omega$	$U_{\text{osc}} = 5 \text{ V}$	$\omega_{ii} = 1.92 \cdot 10^5$	$f_{zi} = 1.8 \text{ kHz}$	$f_{pi} = 34.5 \text{ kHz}$	$f_{ci} = 8.3 \text{ kHz}$

TABLE II - SEPIC CONVERTER PARAMETER VALUES

$U_g = 127 \text{ V}_{\text{RMS}} \pm 20\%$	$U_o = 200 \text{ V}$	$P_o = 600 \text{ W}$	$f_s = 70 \text{ kHz}$		
$L_1 = 650 \mu\text{H}$	$L_2 = 1.1 \text{ mH}$	$C_1 = 0.94 \mu\text{F}$	$C = 330 \mu\text{F}$	$R_d = 68 \Omega$	$C_d = 2.2 \mu\text{F}$
$R_S = 33 \text{ m}\Omega$	$U_{\text{osc}} = 5 \text{ V}$	$\omega_{ii} = 1.62 \cdot 10^5$	$f_{zi} = 1.5 \text{ kHz}$	$f_{pi} = 28.6 \text{ kHz}$	$f_{ci} = 7 \div 12 \text{ kHz}$

TABLE III - COMPARISON BETWEEN MODEL FORECASTS AND EXPERIMENTAL MEASUREMENTS FOR THE BOOST PFP

N°.	OPERATING POINT	FILTER PARAMETERS	EXPERIMENTAL	MODEL I	MODEL II
1	$U_o = 180\text{V}$ $I_o = 2.75\text{A}$	$L_F = 0.89\text{mH}$ $C_F = 0.47\mu\text{F}$	$\hat{U}_g = 119\text{V}$ $f_{\text{osc}} = 17.24\text{kHz}$	$\hat{U}_g = 125\text{V}$ $f_{\text{osc}} = 16.34\text{kHz}$	$f_{\text{cr}} = 16.7\text{kHz}$ $m_\phi = -1.4\text{deg}$
2	$U_o = 220\text{V}$ $I_o = 0.8\text{A}$	$L_F = 1.12\text{mH}$ $C_F = 0.47\mu\text{F}$	$\hat{U}_g = 76.4\text{V}$ $f_{\text{osc}} = 17.86\text{kHz}$	$\hat{U}_g = 71\text{V}$ $f_{\text{osc}} = 17.2\text{kHz}$	$f_{\text{cr}} = 16.6\text{kHz}$ $m_\phi = 2.3\text{deg}$
3	$U_o = 220\text{V}$ $I_o = 1\text{A}$	$L_F = 1.12\text{mH}$ $C_F = 0.47\mu\text{F}$	$\hat{U}_g = 84.4\text{V}$ $f_{\text{osc}} = 18.12\text{kHz}$	$\hat{U}_g = 79.6\text{V}$ $f_{\text{osc}} = 17.2\text{kHz}$	$f_{\text{cr}} = 16.7\text{kHz}$ $m_\phi = 2\text{deg}$
4	$U_o = 220\text{V}$ $I_o = 1.5\text{A}$	$L_F = 1.07\text{mH}$ $C_F = 0.47\mu\text{F}$	$\hat{U}_g = 100\text{V}$ $f_{\text{osc}} = 18.2\text{kHz}$	$\hat{U}_g = 98\text{V}$ $f_{\text{osc}} = 17.2\text{kHz}$	$f_{\text{cr}} = 17\text{kHz}$ $m_\phi = 0.7\text{deg}$
5	$U_o = 220\text{V}$ $I_o = 2\text{A}$	$L_F = 0.89\text{mH}$ $C_F = 0.47\mu\text{F}$	$\hat{U}_g = 118\text{V}$ $f_{\text{osc}} = 18\text{kHz}$	$\hat{U}_g = 115\text{V}$ $f_{\text{osc}} = 17.34\text{kHz}$	$f_{\text{cr}} = 17.13\text{kHz}$ $m_\phi = 0.9\text{deg}$
6	$U_o = 300\text{V}$ $I_o = 1\text{A}$	$L_F = 1\text{mH}$ $C_F = 0.47\mu\text{F}$	$\hat{U}_g = 105\text{V}$ $f_{\text{osc}} = 18.5\text{kHz}$	$\hat{U}_g = 90\text{V}$ $f_{\text{osc}} = 19.3\text{kHz}$	$f_{\text{cr}} = 17.74\text{kHz}$ $m_\phi = 6.1\text{deg}$
7	$U_o = 300\text{V}$ $I_o = 1.5\text{A}$	$L_F = 0.67\text{mH}$ $C_F = 0.47\mu\text{F}$	$\hat{U}_g = 127\text{V}$ $f_{\text{osc}} = 17.86\text{kHz}$	$\hat{U}_g = 114\text{V}$ $f_{\text{osc}} = 19.5\text{kHz}$	$f_{\text{cr}} = 18.5\text{kHz}$ $m_\phi = 4.1\text{deg}$
8	$U_o = 300\text{V}$ $I_o = 2\text{A}$	$L_F = 0.55\text{mH}$ $C_F = 0.47\mu\text{F}$	$\hat{U}_g = 144\text{V}$ $f_{\text{osc}} = 18.2\text{kHz}$	$\hat{U}_g = 136\text{V}$ $f_{\text{osc}} = 19.8\text{kHz}$	$f_{\text{cr}} = 19.2\text{kHz}$ $m_\phi = 2.3\text{deg}$

TABLE IV - COMPARISON BETWEEN MODEL FORECASTS AND EXPERIMENTAL MEASUREMENTS FOR THE SEPIC PFP

N°.	OPERATING POINT	FILTER PARAMETERS	EXPERIMENTAL	MODEL I	MODEL II
1	$U_o = 200\text{V}$ $I_o = 1.11\text{A}$	$L_F = 1.14\text{mH}$ $C_F = 0.47\mu\text{F}$	$\hat{U}_g = 97.6\text{V}$ $f_{\text{osc}} = 18\text{kHz}$	$\hat{U}_g = 91\text{V}$ $f_{\text{osc}} = 17.4\text{kHz}$	$f_{\text{cr}} = 17\text{kHz}$ $m_\phi = 3.7\text{deg}$
2	$U_o = 200\text{V}$ $I_o = 1.69\text{A}$	$L_F = 0.8\text{mH}$ $C_F = 0.47\mu\text{F}$	$\hat{U}_g = 126\text{V}$ $f_{\text{osc}} = 18\text{kHz}$	$\hat{U}_g = 117\text{V}$ $f_{\text{osc}} = 18.1\text{kHz}$	$f_{\text{cr}} = 17.7\text{kHz}$ $m_\phi = 3.5\text{deg}$
3	$U_o = 200\text{V}$ $I_o = 2.25\text{A}$	$L_F = 0.55\text{mH}$ $C_F = 0.47\mu\text{F}$	$\hat{U}_g = 143\text{V}$ $f_{\text{osc}} = 18\text{kHz}$	$\hat{U}_g = 142\text{V}$ $f_{\text{osc}} = 18.9\text{kHz}$	$f_{\text{cr}} = 18.9\text{kHz}$ $m_\phi = 0.3\text{deg}$
4	$U_o = 200\text{V}$ $I_o = 2.94\text{A}$	$L_F = 0.55\text{mH}$ $C_F = 0.47\mu\text{F}$	$\hat{U}_g = 176\text{V}$ $f_{\text{osc}} = 18\text{kHz}$	$\hat{U}_g = 167\text{V}$ $f_{\text{osc}} = 19.3\text{kHz}$	$f_{\text{cr}} = 19\text{kHz}$ $m_\phi = 3\text{deg}$
5	$U_o = 180\text{V}$ $I_o = 1.29\text{A}$	$L_F = 1.1\text{mH}$ $C_F = 0.47\mu\text{F}$	$\hat{U}_g = 100\text{V}$ $f_{\text{osc}} = 18\text{kHz}$	$\hat{U}_g = 95\text{V}$ $f_{\text{osc}} = 17\text{kHz}$	$f_{\text{cr}} = 16.8\text{kHz}$ $m_\phi = 2.3\text{deg}$
6	$U_o = 180\text{V}$ $I_o = 1.54\text{A}$	$L_F = 0.98\text{mH}$ $C_F = 0.47\mu\text{F}$	$\hat{U}_g = 112\text{V}$ $f_{\text{osc}} = 18\text{kHz}$	$\hat{U}_g = 106\text{V}$ $f_{\text{osc}} = 17.3\text{kHz}$	$f_{\text{cr}} = 17\text{kHz}$ $m_\phi = 2.6\text{deg}$
7	$U_o = 168\text{V}$ $I_o = 2.57\text{A}$	$L_F = 0.55\text{mH}$ $C_F = 0.47\mu\text{F}$	$\hat{U}_g = 143\text{V}$ $f_{\text{osc}} = 18\text{kHz}$	$\hat{U}_g = 146\text{V}$ $f_{\text{osc}} = 18.3\text{kHz}$	$f_{\text{cr}} = 18.4\text{kHz}$ $m_\phi = -1\text{deg}$